Vol. 6 • No. 5 • March 8 • 2017

www.advhealthmat.de

ADVANCED HEALTHCARE MATERIALS

WILEY-VCH

Thin, Soft, Skin-Mounted Microfluidic Networks with Capillary Bursting Valves for Chrono-Sampling of Sweat

*Jungil Choi, Daeshik Kang, Seungyong Han, Sung Bong Kim, and John A. Rogers**

Systems for time sequential capture of microliter volumes of sweat released from targeted regions of the skin offer the potential to enable analysis of temporal variations in electrolyte balance and biomarker concentration throughout a period of interest. Current methods that rely on absorbent pads taped to the skin do not offer the ease of use in sweat capture needed for quantitative tracking; emerging classes of electronic wearable sweat analysis systems do not directly manage sweat-induced fluid flows for sample isolation. Here, a thin, soft, "skin-like" microfluidic platform is introduced that bonds to the skin to allow for collection and storage of sweat in an interconnected set of microreservoirs. Pressure induced by the sweat glands drives flow through a network of microchannels that incorporates capillary bursting valves designed to open at different pressures, for the purpose of passively guiding sweat through the system in sequential fashion. A representative device recovers 1.8 µL volumes of sweat each from 0.8 min of sweating into a set of separate microreservoirs, collected from 0.03 cm^2 area of skin with approximately five glands, corresponding to a sweat rate of 0.60 µL min^{-1} per gland. Human studies demonstrate applications in the accurate chemical analysis of lactate, sodium, and potassium concentrations and their temporal variations.

1. Introduction

Sweat, a biofluid excreted by eccrine glands in the epidermis, contains electrolytes (sodium, chloride) along with lactate, urea, and small quantities of proteins, peptides, and metal ions.[1] The concentrations of these and other biomarkers provide important information on physiological state, such as dehydration,[2] and on diseases such as cystic fibrosis[3] and childhood pancreatic disease.[4] Temporal changes and variations in the chemistry of sweat across body positions offer additional insights into health status.[5–9] In this context, wearable devices capable of collecting and storing sweat in discrete chambers have potential value. Established technologies rely on absorbent patches (PharmChek)[10] or coiled tubes (Macroduct),[11] and serve only as passive vehicles for sweat collection over a certain period of time. Capturing samples at different times requires repeated application and removal of such devices.[5–7]

Several forms of wearable, electronic sweat analysis systems exploit electrochemical approaches for monitoring biomarker concentrations, but they do not also allow for collection, capture or subsequent analysis of discrete samples of sweat captured at well-defined time points.[12–21] Emerging flexible microfluidic systems have been developed[22,23] for measuring mechanical forces,[24–26] temperature, and chemical markers such as pH and glucose[27] and for microfluidic drug delivery.[28] Although these devices are capable of sensing biomarkers and delivering liquid agents, they are not designed for capture and storage of sweat using microfluidic control and ex situ analysis. Textile-based microfluic devices platform can direct sweat to chemical sensors,[29,30] using capillary forces from fabric materials as passive pumps, but this type of strategy is incompatible with the time sequential filling capabilities that we introduce here. Our own work establishes foundations for skin-mounted microfluidic systems for quantitative determination of biomarkers via colorimetric analysis.[31] The platform reported here can provide similar capabilities, with additional features in chrono-sampling of sweat, for determination of time dependent variations in biomarkers, and with collection chambers for sweat extraction and ex situ analysis.

This work on thin, soft, skin-mounted microfluidic systems defines routes for exploiting sophisticated concepts in lab-on-a-chip technologies for sweat collection and analysis directly

Dr. J. Choi
Department of Materials Science and Engineering
Northwestern University
Evanston, IL 60208, USA
Prof. D. Kang
Department of Mechanical Engineering
Ajou University
San 5, Woncheon-Dong, Yeongtong-Gu,
Suwon 16499, South Korea
Dr. S. Han, Dr. S. B. Kim
Department of Materials Science and Engineering
Frederick Seitz Materials Research Laboratory
University of Illinois at Urbana-Champaign
Urbana, IL 61801, USA
Prof. J. A. Rogers
Center for Bio-Integrated Electronics
Departments of Materials Science and Engineering,
Biomedical Engineering, Chemistry, Mechanical Engineering,
Electrical Engineering and Computer Science, and Neurological Surgery
Simpson Querrey Institute for Nano/Biotechnology
McCormick School of Engineering and Feinberg School of Medicine
Northwestern University
Evanston, IL 60208, USA
E-mail: jrogers@northwestern.edu

DOI: 10.1002/adhm.201601355

from and on the surface of the skin. Here, sweat glands, which create pressure due to natural differences of osmolality between plasma and sweat,[32] actively drive flow into networks of microchannels and microreservoirs formed in soft elastomers. The maximum pressures generated in this manner are ≈70 kPa per gland,[33] sufficient for this purpose. Although previously reported systems do not incorporate any valves for controlling the direction of flow through the microfluidic network, piezoelectric,[34] electrokinetics,[35] and chemical approaches[36] are compatible with the basic platform, and can be considered for this purpose. Herein, we report an approach that guides flow in these types of skin-mounted microfluidic devices via a collection of carefully designed capillary bursting valves (CBVs) that direct the flow of sweat to fill a collection of microreservoirs in a sequential manner, thereby providing a precise sampling capability. Past works on conventional lab-on-a-chip technologies demonstrate that CBVs can be used for stop valves[37–40] and flow guides,[41,42] but not for the type of control achieved here or for skin-mounted systems. Systematic in vitro tests illustrate robust, stable function in various conformal, skin-compatible designs that additionally allow efficient means for storage and final extraction of discrete samples of sweat. Field testing on human subjects validates the utility of platforms configured for sequential sweat sampling followed by extraction and ex situ chemical analysis, with a focus on lactate, sodium, and potassium. These initial studies indicate differences between sweat generated by thermal exposures and by running exercises, as well as variations with position across the body.

2. Results and Discussion

2.1. Thin, Soft Microfluidic Devices for Chrono-Sampling of Sweat

The thin geometries and soft mechanics of these devices allows their intimate, comfortable bonding to the skin for the purpose of collecting, manipulating, analyzing, and storing sweat, captured in a sequential manner. A representative device shown in **Figure 1**a has a circular overall geometry with a diameter of 3 cm. The radial construction facilitates the use of centrifugation techniques for collection of sweat after removing the device from the skin, as described subsequently. The design involves two layers of poly(dimethylsiloxane) (PDMS) supported on a medical-grade acrylic adhesive film for bonding to the skin. The first layer defines a network of microfluidic channels (400 μm thickness; channel widths and heights are 200 and 300 μm, respectively) and the CBVs (designs described next). The second serves as a capping layer (200 μm thickness; inlet), and the third (50 μm thickness) establishes adhesion to the skin and defines openings (2 mm diameter) from which sweat can enter the microfluidic system (1 mm diameter, inlet; Figure 1b and Figure S1, Supporting Information). The structure in Figure 1 consists of a network of microfluidic channels that connects to 12 separate chambers in parallel by bridging channels (Figure 1c). Each chamber connects to an outlet opening (0.5 mm diameter) designed to allow release of air that would otherwise be trapped in the chamber and serve as a source of backpressure to frustrate the filling of sweat into the chamber.

In vitro tests using dyed water illustrate the clockwise flow through this network (Figure 1d). PDMS is a good choice due to its dimensional stability in water,[43] materials biocompatibility,[44] low modulus, elastic mechanical properties, and compatibility with simple molding and bonding processes for fabrication.[45–47] Previous studies show that amino acids, glucose, and pyruvate exhibit low absorption into PDMS. Other chemistries, including certain vitamins and hormones, have comparatively high absorption, but their concentrations are generally not crucial to analysis of sweat.[44,48] Careful testing indicates an absence of chemical contamination from the PDMS and the adhesive layer in analysis of biomarkers of interest in sweat (Figure S2, Supporting Information). These same results suggest a minor (≈10%) decrease in glucose concentration, possibly due to slight absorption into the constituent materials of the device.

2.2. Principle and Design of the Capillary Bursting Valves for Sequential Sampling

The CBVs block flows at pressures lower than their characteristic bursting pressures (BPs).[49] When liquid in a single connected channel encounters two separate CBVs with different BPs, at sufficient pressures, the flow will proceed first through the valve with lower BP. In this way, locating two CBVs with different BPs near the intersection between two channels allows control of the direction of flow. The Young–Laplace equation gives the BP in a rectangular channel as[49,50]

$$\mathrm{BP} = -2\sigma\left[\frac{\cos\theta_{\mathrm{I}}^{*}}{b} + \frac{\cos\theta_{\mathrm{A}}}{h}\right] \quad (1)$$

where σ is the surface tension of liquid, θ_{A} is the contact angle of the channel, θ_{I}^{*} is the $\min[\theta_{\mathrm{A}} + \beta; 180°]$, β is the diverging angle of the channel, b and h are the width and the height of the diverging section, respectively. For hydrophobic materials at high diverging angles, the BP increases with decreasing b and h. Each unit cell of the devices described here includes three CBVs, a collection chamber, an extraction chamber and a sampling outlet (**Figure 2**a). In one embodiment, the first two CBVs, denoted #1 and #2, have diverging angles of 13° and 90°, respectively, and widths of 200 μm. The third CBV, i.e., #3, has a diverging angle of 120° and a width of 50 μm (Figure 2b). The heights of the valves are 300 μm. According to Equation (1), the contact angle of the channel surfaces affects the BP. PDMS, which is naturally hydrophobic, becomes hydrophilic after exposure to oxygen plasma for the purpose of activating the surfaces to enable bonding. The hydrophobicity recovers after ≈24 h, to reach a constant, time-independent contact angle of 107°.[51] Based on this parameter, the computed BPs for CBVs #1, #2, and #3 are 498.9 (BP #1), 881.7 (BP #2), and 3035.7 Pa (BP #3), respectively. Experimentally measured values are somewhat lower than these estimates, mainly due to imperfections in the fabrication and, in particular, diverging angles that are slightly smaller than the design values, as shown in the SEM images in Figure 2a.[49] For example, in CBV #2 and #3, the sharp edges where the straight channel and the diverging section intersect are

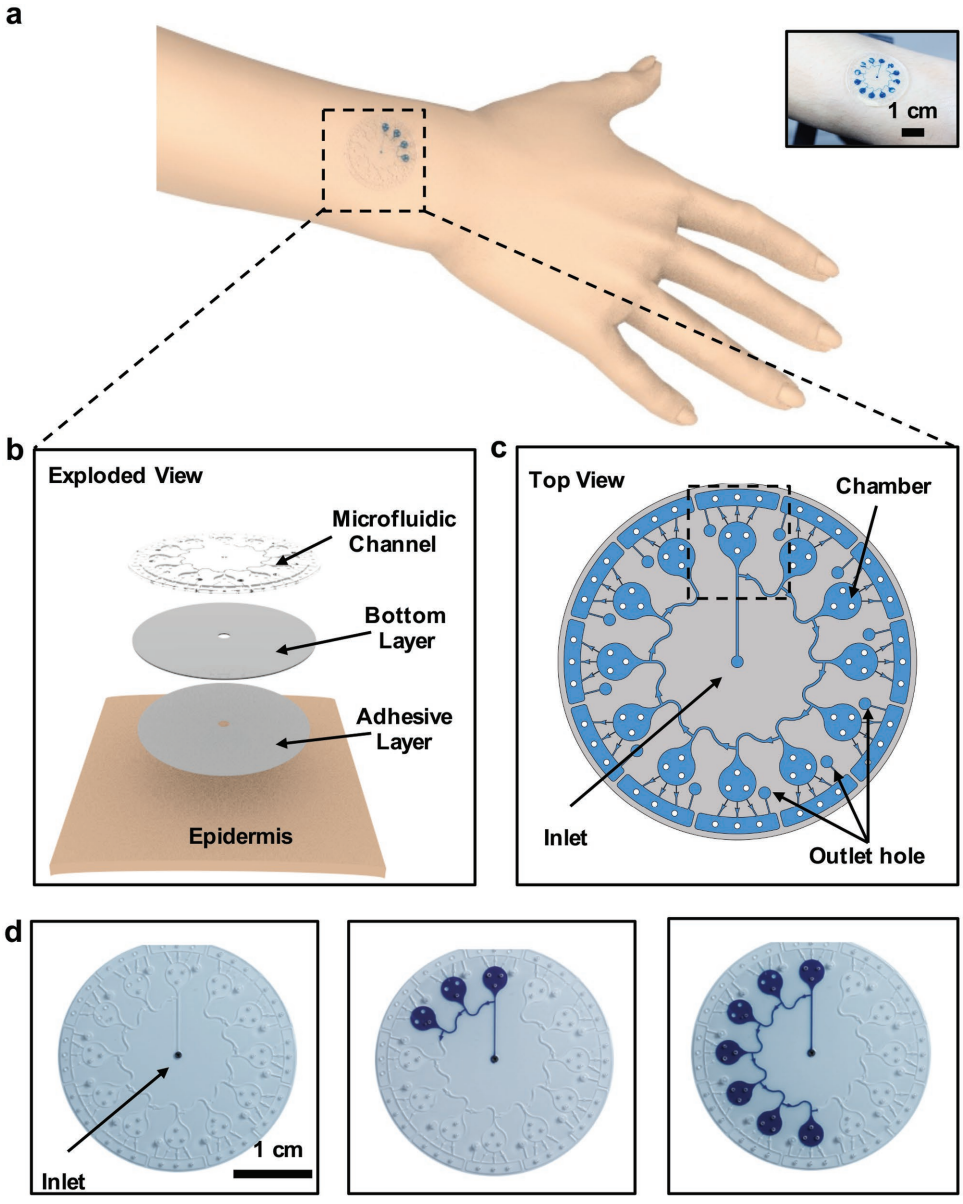

Figure 1. a) Schematic illustrations and optical images (inset) of thin, soft microfluidic devices for chrono-sampling of sweat. b) Exploded view illustration of a device and its interface with skin. c) Top view illustration of microfluidic channels filled with blue-dyed water. d) Optical images of in vitro testing of chrono-sampling of blue-dyed water in a working device.

somewhat rounded, with radii of curvature of ≈35 and 27 μm, respectively (Figure S3, Supporting Information).

Liquid that initially arrives at CBVs #1 and #2 encounters them in their closed states (Figure 2e(i)). Upon reaching or exceeding BP #1, CBV #1 opens to allow flow into the chamber (Figure 2e(ii)). After filling this chamber, the liquid flow bursts CBV #2 at sufficient pressure (BP of CBV #2 is lower than that of CBV #3) (Figure 2e(iii)). By this process, all 12 chambers fill in a sequential manner, for flows that involve pressures larger than BP #2. Due to the pressure drop along the channel, the required pressure to fill the whole chambers is ≈1000 Pa and is higher than BP #2 (Figure S4, Supporting Information). For constant flow rate, this effect translates to time-sequenced sampling, or chrono-sampling. After use, the device can be removed from the skin and then inserted into a centrifuge (5000 rpm) to open CBV #3, thereby moving liquid from each of the storage chambers into corresponding extraction chambers to facilitate recovery for lab analysis (Figure 2e(iv)). The designs of the CBVs ensure that pressures generated by the sweat glands exceed BP #1 and BP #2, thereby allowing complete filling of the associated chambers, and that centrifugal pressures exceed BP #3. The pressure generated by the sweat glands exceeds BP #3, but it does not burst this valve until after filling the chamber. (Thick, high areal coverage of hair can, potentially lead to lateral leakage. Our studies did not uncover significant problems, but advanced, conformal adhesive layers could be implemented to minimize such effects in cases where they are important.)

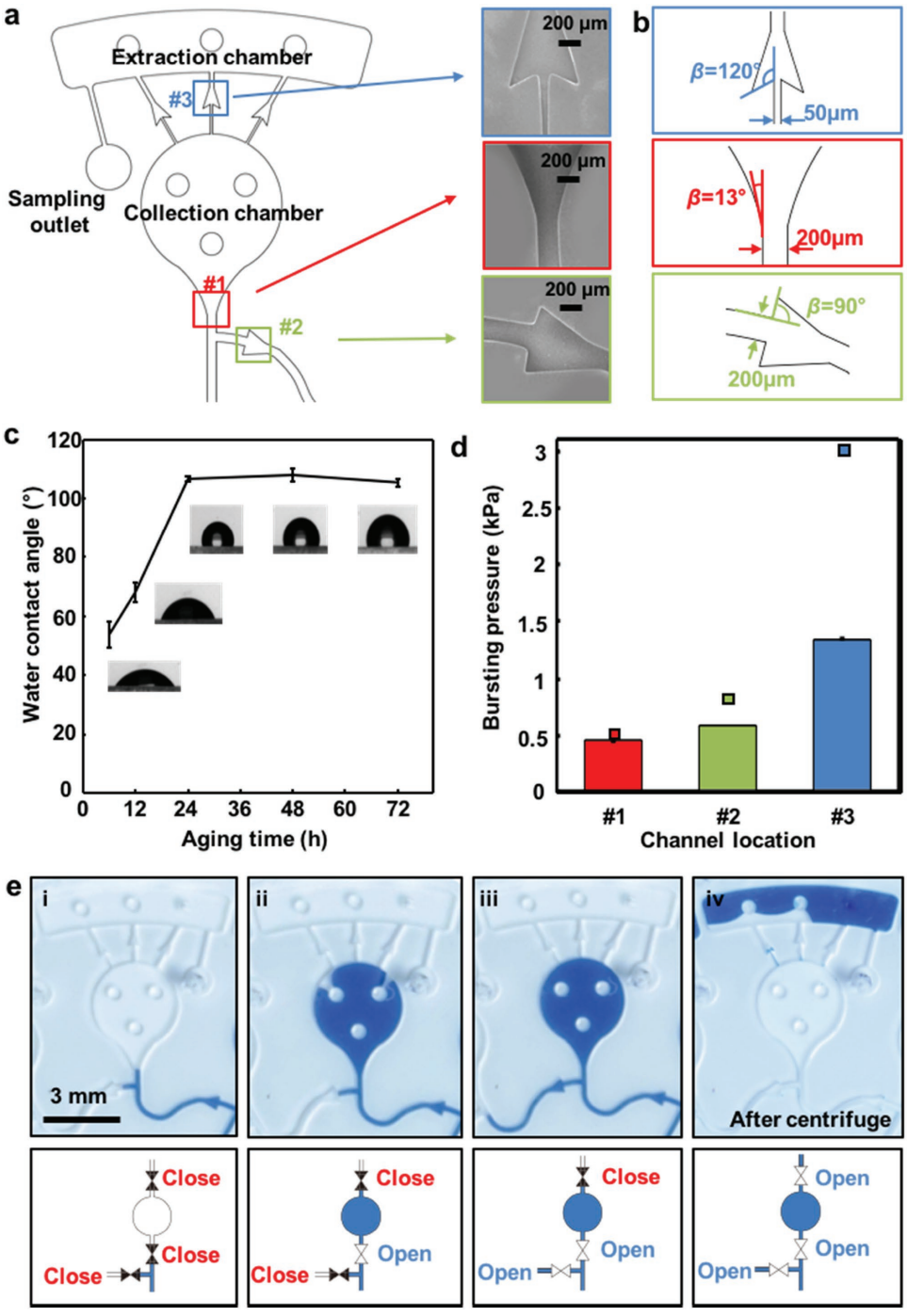

Figure 2. a) Detailed schematic illustration of a unit cell in a device, including a collection chamber, extraction chamber, sampling outlet, and three capillary bursting valves (CBV) and SEM images of CBVs. b) Sketch of capillary bursting valves with indicated channel width and diverging angle. c) Measurement of contact angle of water on PDMS as a function of aging time after oxygen plasma treatment. d) Experimental results (bars) and theoretical values (square box) of capillary bursting pressure of CBV #1, #2, and #3 of device after 1 day from oxygen plasma treatment. e) Optical images and schematic illustrations of the working principle of the capillary bursting valves for chrono-sampling. (i) Before entering collection chamber (ii) filling the collection chamber (iii) flowing to next chamber (iv) after centrifugation.

2.3. Fluidic Operation and Stability under Mechanical Perturbation

Figure 3a shows that these epidermal microfluidic chrono-sampling devices can sequentially collect liquid without undesired bursting of CBVs (Movie S1, Supporting Information). The flow properties of the microchannels ensure absence of unwanted mixing. Specifically, for channel dimensions of hundreds of micrometers and flow rates up to 1.0 μL min^{-1} in the device, the flows are laminar, i.e., low Reynolds numbers

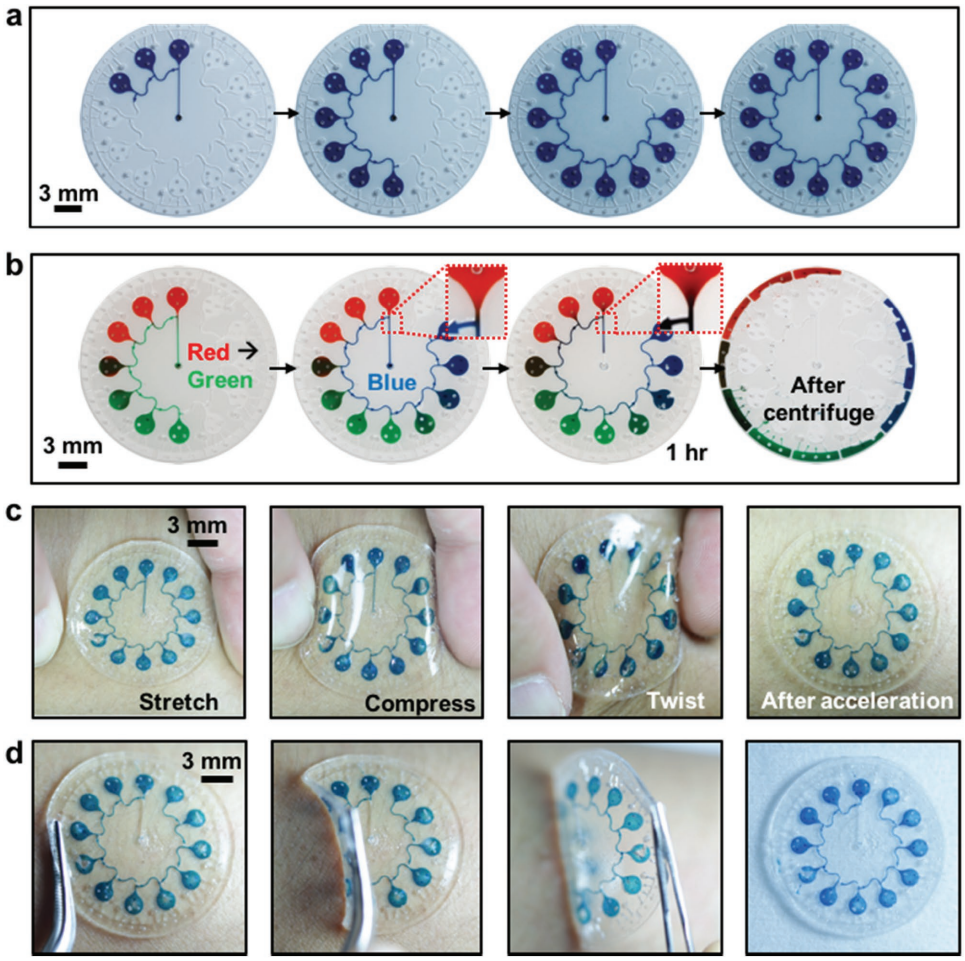

Figure 3. Optical images of a) in vitro testing of chrono-sampling with dyed water in a device with 12 chambers, b) in vitro testing of chrono-sampling with different colored dyes in water (red, green, and blue) and enlarged images of the interface between different colored dye and after separation using centrifugation, c) epidermal microfluidic chrono-sampling devices filled with dyed water and attached to the skin during various modes of mechanical distortion and motion: stretch, compress, twist, and acceleration, d) demounting of a device filled with dyed water and attached to the skin.

(<1), and mixing occurs only by molecular diffusion.[52,53] The example here illustrates operation with water dyed using different colors and introduced in a time sequenced manner. Over relevant time scales (≈1 h) and temperatures (≈22 °C), diffusion occurs only within ≈1 mm of the interfaces between water with different colors, corresponding to less than 10% of the total volume of the collection chamber. The fourth chamber in this example is relatively dark due to mixing of the red dye in the bridge channel with green dye. Here, the red dye comes from the inlet and green dye follows the red, in sequence.

After filling 11 chambers, removing the device and performing centrifugation, each separate sample of sweat moves into a corresponding extraction chamber. Figure 3c highlights the soft nature of these devices and their ability to stretch, flex, and twist without damage. The function of the microfluidic channels, CBVs, and chambers is unaffected by these deformations or by shaking movements of the arm. Even the process of removing the device from the skin for chemical analysis, which includes significant mechanical stresses, does not affect the stability or fluidic containment (Figure 3c,d).

2.4. Various Design Features of Epidermal Microfluidic Sweat Chrono-Sampling Devices

These device platforms offer significant design versatility in terms of overall dimensions, sizes of microfluidic channels and chambers, and numbers of chambers, as illustrated in **Figure 4**a. The smallest device shown here has three chambers, and a circular layout with a diameter of 1 cm, for use in space constrained regions such as behind the ear. Due to the thin, soft mechanical construction, this device and others with different designs can mount on various locations on the body with equal fidelity, including the chest, back, forearm, and thigh (Figure 4b). Additional features can be included. For example, in a standard layout, the adhesive covers the skin everywhere except regions for collecting sweat. Possible effects related to blockage of sweat glands (i.e., compensatory sweating) can be reduced with the addition of channels of relief on the bottom surface of the device to define skin-interfaced microfluidic channels for transport of sweat to the outer perimeter (Figure 4c and Figure S5a,b, Supporting Information). Another option involves the introduction of open architectures via removal of regions of

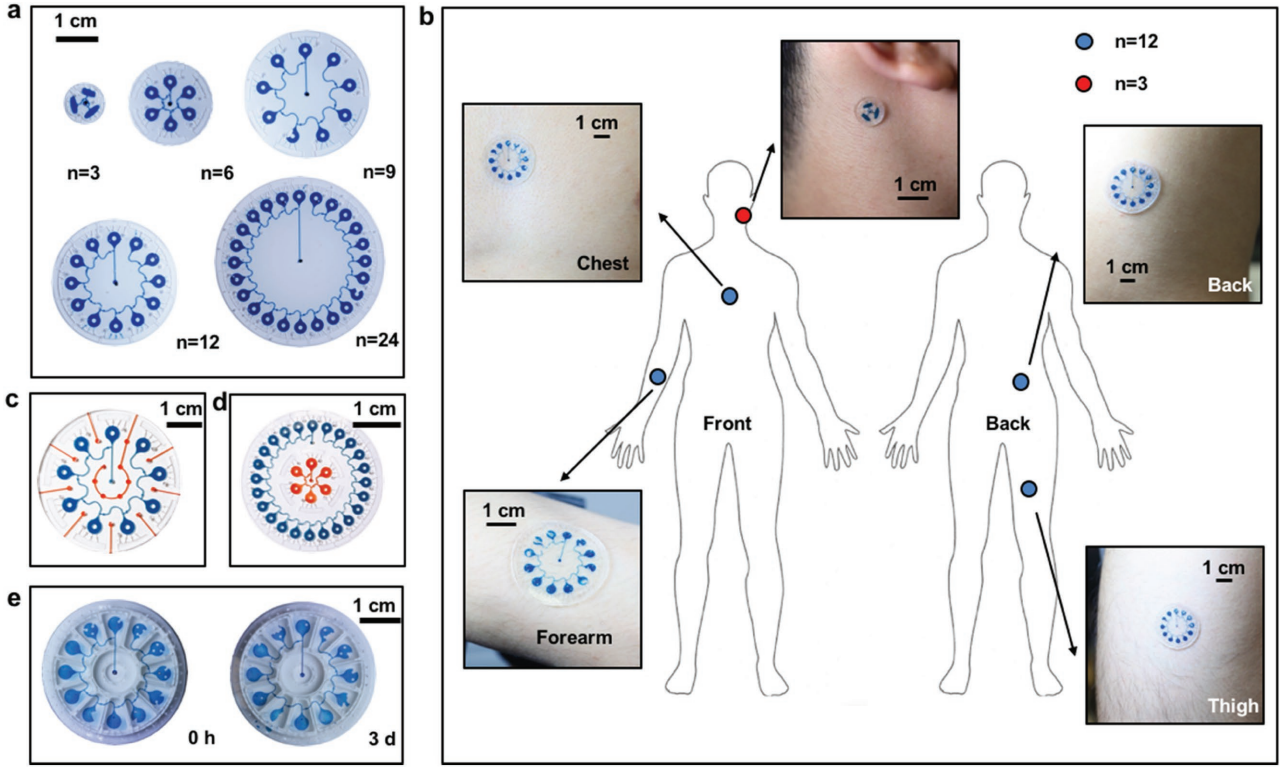

Figure 4. Optical images of a) devices with various sizes and numbers of chambers of filled with dyed water. The sizes are from 1 to 4 cm and the number of chambers are from 3 to 24, b) various mounting positions on the body; behind the ear, chest, back, forearm, and thigh, c) devices with sweat guiding channels, d) devices with another set of sampling chambers at the center, e) device after sampling of dyed water (0 h) and after 3 days of storage using an evaporation blocking clamp in high humidity conditions.

the device where the skin adhesive interface is not necessary (Figure S5c, Supporting Information). Such layouts improve not only management of flows of sweat in these locations but they also increase the mechanical deformability. For the largest device, it is possible to locate an additional set of sampling capabilities in the center region (Figure 4d). The volume of the chamber can also be defined to meet requirements, with examples of 2.3 and 6.1 μL in Figure S5d (Supporting Information).

The microscale dimensions of the devices, the water permeability of PDMS and the presence of microchannels and chambers with open outlets collectively lead to non-negligible rates of evaporation of sweat during and after use. Experiments show that the evaporation rate from a typical device is ≈3.5 μL h^{-1} in a fully filled state, which equates to a perchamber rate of ≈0.25 μL h^{-1} at 35 °C, 40% relative humidity (Figure S6a, Supporting Information). This rate corresponds to ≈10 % of the chamber volume per hour. Systematic studies show that most evaporation occurs through the sample outlets (Figure S6c, Supporting Information). For long-term storage, mechanical clamps designed to block these regions (Figure S6c–e, Supporting Information) reduce the rate to 0.55 μL h^{-1} in a fully filled state and 0.04 μL h^{-1} per chamber at 25 °C, 30% relative humidity such that more than 50% of the samples can be retained in the device for 1 day. Storage in high humidity conditions (99%) is possible for several days (Figure 4d). In addition, proteins and peptides in the sweat can enzymatically degradation in a few hours at room temperature.[54] To prevent such degradation, hydrogel nanoparticles containing high affinity reactive chemical baits could be incorporated into the storage reservoirs.[55]

2.5. In Situ Chrono-Sampling and Chemical Analysis of Sweat Samples in Human Trials

Human testing involved evaluations on volunteer subjects during running exercises and sessions in a sauna room. A formulation of $CoCl_2$ in polyhydroxyethylmethacrylate (pHEMA) coats the center regions of the chambers to produce a color change upon contact with sweat, thereby facilitating visualization of the filling process. For a representative running test, the first chamber filled after 8 min 20 s and the last chamber filled 10 min later (**Figure 5**a). In a sauna, the first chamber filled after 13 min 33 s and the last chamber filled after 8 min 30 s (Figure 5b). In both cases, the time for filling each chamber after the first is less than one minute. At the inlet (2 mm in diameter), there are approximately five sweat glands. In the running exercise, the average sweat rate from the initiation of sweating to complete filling of the chambers is 0.60 μL min^{-1} per gland. In the sauna, corresponding values are 0.65 μL min^{-1} per gland. The main difference between these two cases is that the initiation of sweating is delayed in the sauna. These values are significantly higher than those measured using absorbent pads[56] (Figure S7a,b, Supporting Information), due mainly to

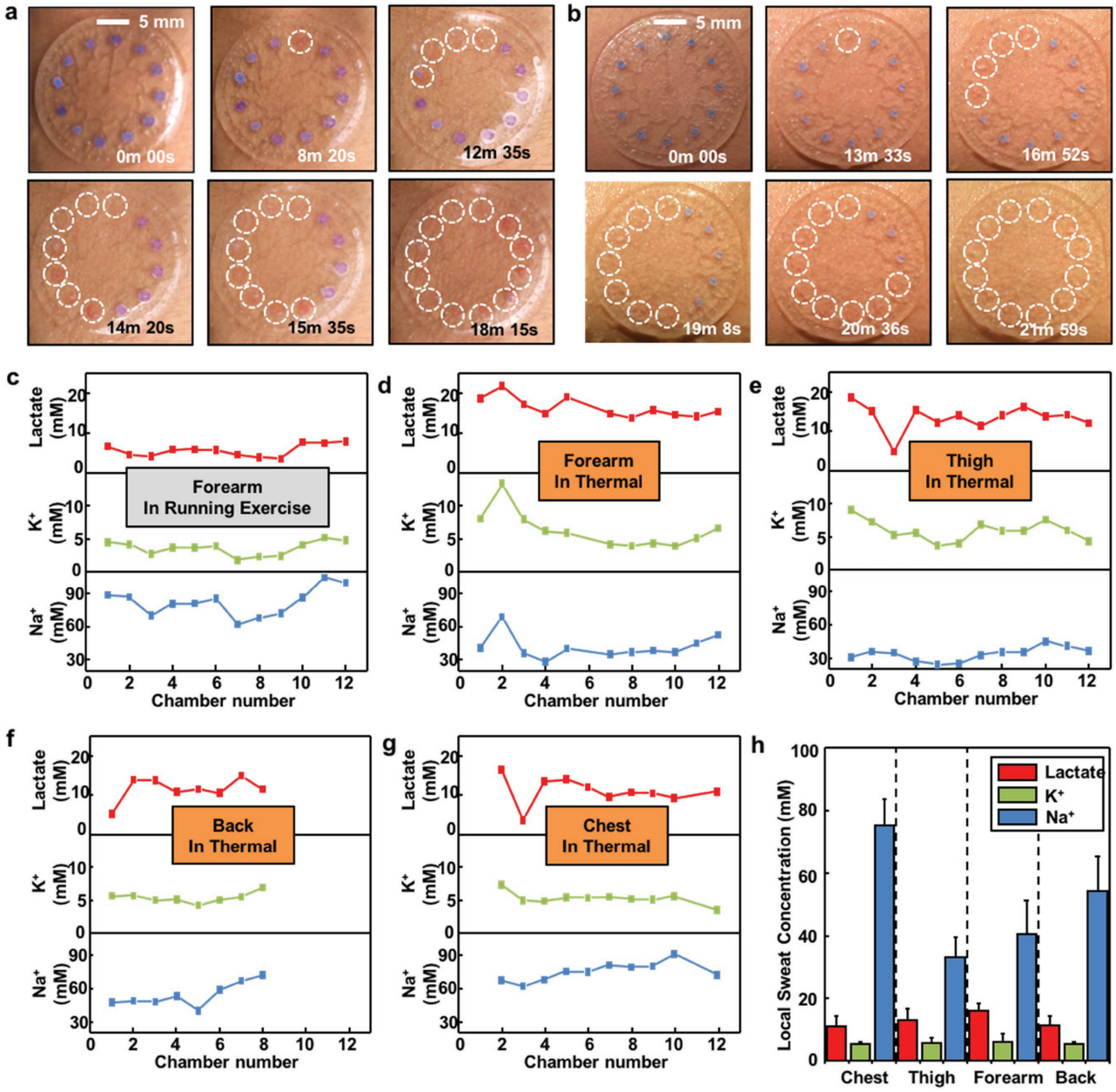

Figure 5. In situ chrono-sampling from various body positions during running exercise and thermal exposure, along with chemical analysis of captured sweat samples. Sweat chrono-sampling from the forearm a) in running exercise at constant speed b) in thermal exposure at 56 °C. Chemical analysis of lactate, sodium, and potassium of sweat from a chrono-sampling device from c) forearm in running exercise, d) from forearm, e) thigh, f) back, and g) chest in thermal exposure. h) Regional variations of sweat concentration (lactate, sodium, and potassium) from different body positions; chest, thigh, forearm, and back.

compensatory effects associated with adjacent regions of the skin that are blocked from release of sweat by the presence of the device.[57] A simple test with adhesive tape shows significantly more sweat at the edges of the tape than at the adjacent regions of the bare skin (Figure S7c, Supporting Information). In the device used for studies described above, the inlet region consists of a circular region with area of ≈3 mm^2, where sweat enters the microfluidic system, and a surrounding area of ≈700 mm^2 where the adhesive bonds to the skin. Compensatory effects can be reduced and nearly eliminated by the addition of interfacial channels, as described previously, that allow the release of sweat from regions adjacent to the inlet, for transport to the device periphery (Figure 4c and Figure S5a,b, Supporting Information). With this type of design, measurements of sweat rate and sweat loss can lie within a factor of two of those measured using absorbent pads (Figure S7d, Supporting Information).

Centrifugation and retrieval of samples from the extraction chambers of devices without $CoCl_2$/pHEMA allows mass spectrometer analysis of the concentrations of key biomarkers. 80%

of sweat in the chamber can be recovered for further analysis. This approach does not enable analysis of glucose, urea, calcium, and magnesium because microliter sample volumes with analytes at physiologically relevant ranges of concentration fall below limits of detection for the lab analytical instruments available for the present work. The microfluidic device designs described here extract relatively small amounts of sweat compared to the total sweat released from the region of the skin defined by the overall device geometry. Comparisons between compositions of sweat collected from a device configured to capture much larger volumes (300 µL) and from harvesting sweat directly using conventional methods reveal no significant differences (Figure S8, Supporting Information). For devices mounted on the forearm, samples collected after a running exercise indicate a systematic decrease in lactate concentration for chambers 1–9, followed by a slight increase for chambers 10–12 (Figure 5c). The concentration of sodium remains constant until chamber 6, decreases for chamber 7 and then increases again throughout. The decrease in concentration of lactate is consistent with the known dilution effect with increased sweating.[33] The overall concentration of lactate is higher for sweat generated by sauna exposure compared to running, and the reverse trend applies for sodium (Figure 5d); both observations are consistent with previous studies using primitive sweat harvesting techniques.[6]

The applicability of the epidermal microfluidic systems to locations across the body allows, as an example, comparisons of sweat from forearm, thigh, back, and chest (Figure 5d–g). Sodium and lactate are more concentrated in the sweat collected from the chest and forearm (Figure 5h), respectively, in agreement with findings obtained with other approaches.[58–60] The data reveal no substantial differences in potassium concentration for these body positions. Interestingly, in all cases, peaks in concentration often occur at chambers 2 or 3, corresponding to the initial stages of sweating (Figure 5d,e and g). This behavior might be explained by differences in biomarker concentrations between sweat stored in the glands and newly generated sweat. Alternatively, these changes may indicate underlying physiological variations. Previous technologies, due to their lack in volumetric and/or temporal precision, do not allow observation of subtle effects such as these. Even the most sophisticated wearable electronic systems for sweat analysis do not separate the sweat with time, such that sweat released at different times mixes together at the point of measurement.[12–18]

In addition, contamination of sweat can follow from interaction with the epidermis.[5] The analytes explored here are not significantly affected by this form of contamination, but protein, glucose, calcium, and urea concentrations can be altered, especially in the sweat samples collected at or near the onset of sweating. For the wide application of this device, application of mineral oil on the skin could be an appropriate solution for obtaining sweat samples least contaminated at the sweat-epidermal interface.[61]

3. Conclusion

In summary, this paper introduces a soft, thin, skin-compatible, or "epidermal," microfluidic device platform for sequential capture, storage, and retrieval of microliter volumes of sweat. A key advance is in the development and use of microfluidic capillary bursting valves tailored to operate in a range of pressures commensurate with those naturally generated by sweat glands in human skin. Trials on volunteer subjects in various scenarios and regions of the body reveal temporal and spatial changes in the concentration of key biomarkers. The results suggest interesting time-dependent processes of relevance to exercise physiology and health/wellness more generally. Combined use of these platforms with colorimetric schemes for chemical sensing and with epidermal electronic components provides a broad range of engineering options in the design of advanced systems of relevance for personal and clinical applications.

4. Experimental Section

Device Fabrication: Fabrication of molds began with spin coating a 15 µm thick film of photoresist (KMPR 1010) on a silicon wafer (Figure S1, Supporting Information). After photolithography, deep reactive ion etching (STS Pegasus ICP-DRIE, SPTS Technologies Ltd.) created trenches in the silicon to a depth of 300 µm. Spin coating formed thin layer of poly(methylmethacrylate) (PMMA; Microchem, MA, USA) on the resulting mold. Pouring PDMS (at a 30:1; Sylgard 184, Dow corning, MI, USA) onto the PMMA film and then spin coating at 200 rpm yielded a thin (400 µm) layer. A mechanical punch tool defined holes with ≈1 mm diameters at the outlet hole of each of the extraction chambers. For the capping layer, pouring PDMS (30:1) into a polystyrene petri dish (VWR, IL, USA) and then spin coating at 400 rpm formed an isolated film (200 µm). As before, a mechanical punch tool defined a hole with 1 mm diameter located at the center of this layer. After exposure to oxygen plasma generated at low power (6.8 W) RF at 500 mTorr (Plasma Cleaner PDC-32G, Harrick Plasma, NY, USA) for 10 s, the channel part and capping layer were aligned and bonded. Aging the bonded structure for 24 h allowed the PDMS surfaces to recover their hydrophobic properties. Bonding to a skin adhesive (PC2723U, ScapaHealthcare) with a 2 mm diameter hole aligned to the inlet completed the fabrication. Introduction of a solution of 100 mg mL^{-1} cobalt (II) chloride dissolved in a 2 wt% pHEMA hydrogel (Sigma-Aldrich, MO, USA) into the channels facilitated visualization of the filling process.

In Vitro Chrono-Sampling Test and Measurement of Bursting Pressure: A hydrostatic pressure generator served as the basis for a simple in vitro model of sweat generation, for the purpose of characterizing the CBVs (Figure S1a, Supporting Information). The height of the top of a water column at the bursting point provided an estimate of the BP. As calibration, the pressure created by the generator was compared to the value from a microfluidic pressure controller (Fluigent MFCS, Villejuif, France).

In Situ Chrono-Sampling Test: Application of ethanol swabs cleaned the skin of volunteers involved in the studies, shortly before application of the devices. For the thermal exposure tests, the subjects remained in a dry sauna at 55 °C for 30–40 min. For the running exercises, the subjects ran at ≈10 km h^{-1} for 30–40 min. After the tests, the devices were peeled from the skin and centrifuged at 5000 rpm to move sweat from the collection chambers into corresponding extraction chambers. For measuring sweat rate by conventional method, hydrophilic foam dressing (Covidien, MA, USA) in 2 cm × 2 cm size was used.

Chemical Contamination Test: Tests for chemical contamination of sweat by constituent materials in the devices used a PDMS channel 2 mm in width and 0.5 mm in depth with a PDMS cover and an adhesive, in an overall construction identical to that of the actual devices (Figure S2a, Supporting Information). Artificial sweat consisted of an aqueous solution of 22×10^{-3} M of urea, 2.2×10^{-3} M of glucose, 3.8×10^{-3} M of potassium, 31×10^{-3} M of sodium, 58×10^{-3} M of chloride, and 5.2×10^{-3} M of calcium (Sigma-Aldrich, MO, USA). This fluid filled

the PDMS channel and remained there for 2 h at room temperature prior to recovery for chemical analysis. A similar sample, without exposure to the test structure, served as a control.

Chemical Analysis: Analysis of lactate involved 1 µL of sweat extracted from the device and subsequently diluted in 100 µL of water. This sample was introduced into liquid chromatography–mass spectrometry system (Waters Synapt G2-Si ESI, MA, USA) with an ACQUITY UPLC BEH C18 column (130 Å, 1.7 µm, 2.1 mm × 50 mm) at a flow rate of 0.2 mL min^{-1}. Solvent A was 95% water, 5% acetonitrile, and 0.1% formic acid; solvent B was 95% acetonitrile, 5% water, and 0.1 % formic acid. Sodium and potassium analysis used 0.5 µL of sweat extracted from the device and subsequently diluted in 1 mL of water. The sweat sample, along with three standard samples (10, 20, and 50 ppb) of sodium and potassium to define a calibration curve, were diluted in 2 mL of 0.5% nitric acid as preparation for inductively coupled plasma mass spectrometry (ICP/MS; SCIEX ELAN DRCe, PerkinElmer, CT, USA). The limit of detection was 1 ppb. For chloride analysis, 1 mL of artificial sweat diluted in 25 mL of water and the 20 mL of solution were mixed with 0.4 mL of 5 M sodium nitrate as ionic strength and pH adjuster (Cat. 940011, Thermo Scientific, MA, USA) to create a uniform background ionic strength. An ion selective electrode was used for measuring chloride concentration (Thermo Scientific, MA, USA).

Contact Angle Measurement: Static contact angles were measured using 5 µL droplets of deionized water dispensed using an automated system and measured with a contact angle goniometer (KSV CAM200, Stockholm, Sweden). Contact angles were evaluated after 10 s of contact. The results establish the kinetics of recovery of hydrophobic properties of the PDMS surface.

Supporting Information

Supporting Information is available from the Wiley Online Library or from the author.

Acknowledgements

J.C. and D.K. contributed equally to this work. This work was supported by the Air Force Research Laboratory. D.K. acknowledges the support from the new faculty research fund of Ajou University and Basic Science Research Program through the National Research Foundation of Korea (NRF) funded by the Ministry of Science, ICT & Future Planning (2016R1C1B1009689).

Received: November 23, 2016
Revised: December 5, 2016
Published online: January 20, 2017

[1] A. Mena-Bravo, M. D. Luque de Castro, *J. Pharm. Biomed. Anal.* **2014**, *90*, 139.
[2] D. B. Dill, D. L. Costill, *J. Appl. Physiol.* **1974**, *37*, 247.
[3] L. E. Gibson, R. E. Cooke, *Pediatrics* **1959**, *23*, 545.
[4] P. A. di Sant'Agnese, R. C. Darling, G. A. Perera, E. Shea, *Am. J. Med.* **1953**, *15*, 777.
[5] T. C. Boysen, S. Yanagawa, F. Sato, K. Sato, *J. Appl. Physiol.: Respir., Environ. Exercise Physiol.* **1984**, *56*, 1302.
[6] T. Fukumoto, T. Tanaka, H. Fujioka, S. Yoshihara, T. Ochi, A. Kuroiwa, *Clin. Cardiol.* **1988**, *11*, 707.
[7] A. K. Shamsuddin, S. Yanagimoto, T. Kuwahara, Y. Zhang, C. Nomura, N. Kondo, *Eur. J. Appl. Physiol.* **2005**, *94*, 292.
[8] R. van Heyningen, J. S. Weiner, *J. Physiol.* **1952**, *116*, 395.
[9] N. A. S. Taylor, C. A. Machado-Moreira, *Extreme Physiol. Med.* **2013**, *2*, 4.
[10] D. A. Kidwell, F. P. Smith, *Forensic Sci. Int.* **2001**, *116*, 89.
[11] K. B. Hammond, N. L. Turcios, L. E. Gibson, *J. Pediatr.* **1994**, *124*, 255.
[12] A. J. Bandodkar, V. W. Hung, W. Jia, G. Valdes-Ramirez, J. R. Windmiller, A. G. Martinez, J. Ramirez, G. Chan, K. Kerman, J. Wang, *Analyst* **2013**, *138*, 123.
[13] T. Guinovart, A. J. Bandodkar, J. R. Windmiller, F. J. Andrade, J. Wang, *Analyst* **2013**, *138*, 7031.
[14] A. J. Bandodkar, D. Molinnus, O. Mirza, T. Guinovart, J. R. Windmiller, G. Valdes-Ramirez, F. J. Andrade, M. J. Schoning, J. Wang, *Biosens. Bioelectron.* **2014**, *54*, 603.
[15] J. Kim, W. R. de Araujo, I. A. Samek, A. J. Bandodkar, W. Z. Jia, B. Brunetti, T. R. L. C. Paixao, J. Wang, *Electrochem. Commun.* **2015**, *51*, 41.
[16] W. Gao, S. Emaminejad, H. Y. Nyein, S. Challa, K. Chen, A. Peck, H. M. Fahad, H. Ota, H. Shiraki, D. Kiriya, D. H. Lien, G. A. Brooks, R. W. Davis, A. Javey, *Nature* **2016**, *529*, 509.
[17] S. Imani, A. J. Bandodkar, A. M. Mohan, R. Kumar, S. Yu, J. Wang, P. P. Mercier, *Nat. Commun.* **2016**, *7*, 11650.
[18] H. Y. Nyein, W. Gao, Z. Shahpar, S. Emaminejad, S. Challa, K. Chen, H. M. Fahad, L. C. Tai, H. Ota, R. W. Davis, A. Javey, *ACS Nano* **2016**, *10*, 7216.
[19] X. Huang, Y. Liu, K. Chen, W. J. Shin, C. J. Lu, G. W. Kong, D. Patnaik, S. H. Lee, J. F. Cortes, J. A. Rogers, *Small* **2014**, *10*, 3083.
[20] B. Schazmann, D. Morris, C. Slater, S. Beirne, C. Fay, R. Reuveny, N. Moyna, D. Diamond, *Anal. Methods* **2010**, *2*, 342.
[21] D. P. Rose, M. E. Ratterman, D. K. Griffin, L. Hou, N. Kelley-Loughnane, R. R. Naik, J. A. Hagen, I. Papautsky, J. C. Heikenfeld, *IEEE Trans. Biomed. Eng.* **2015**, *62*, 1457.
[22] J. C. Yeo, Kenry, C. T. Lim, *Lab Chip* **2016**, *16*, 4082.
[23] J. Heikenfeld, *Electroanalysis* **2016**, *28*, 1242.
[24] J. C. Yeo, J. Yu, M. Shang, K. P. Loh, C. T. Lim, *Small* **2016**.
[25] J. C. Yeo, Kenry, J. H. Yu, K. P. Loh, Z. P. Wang, C. T. Lim, *ACS Sens.* **2016**, *1*, 543.
[26] J. C. Yeo, J. H. Yu, Z. M. Koh, Z. P. Wang, C. T. Lim, *Lab Chip* **2016**, *16*, 3244.
[27] P. Mostafalu, M. Akbari, K. A. Alberti, Q. Xu, A. Khademhosseini, S. R. Sonkusale, *Microsyst. Nanoeng.* **2016**, *2*, 16039.
[28] J. W. Jeong, J. G. McCall, G. Shin, Y. Zhang, R. Al-Hasani, M. Kim, S. Li, J. Y. Sim, K. I. Jang, Y. Shi, D. Y. Hong, Y. Liu, G. P. Schmitz, L. Xia, Z. He, P. Gamble, W. Z. Ray, Y. Huang, M. R. Bruchas, J. A. Rogers, *Cell* **2015**, *162*, 662.
[29] D. Morris, S. Coyle, Y. Z. Wu, K. T. Lau, G. Wallace, D. Diamond, *Sens. Actuators, B* **2009**, *139*, 231.
[30] V. F. Curto, S. Coyle, R. Byrne, N. Angelov, D. Diamond, F. Benito-Lopez, *Sens. Actuators, B* **2012**, *175*, 263.
[31] A. Koh, D. Kang, Y. Xue, S. Lee, R. M. Pielak, J. Kim, T. Hwang, S. Min, A. Banks, P. Bastien, M. C. Manco, L. Wang, K. R. Ammann, K.-I. Jang, P. Won, S. Han, R. Ghaffari, U. Paik, M. J. Slepian, G. Balooch, Y. Huang, J. A. Rogers, *Sci. Transl. Med.* **2016**, *8*, 366ra165.
[32] I. J. Schulz, *J. Clin. Invest.* **1969**, *48*, 1470.
[33] Z. Sonner, E. Wilder, J. Heikenfeld, G. Kasting, F. Beyette, D. Swaile, F. Sherman, J. Joyce, J. Hagen, N. Kelley-Loughnane, R. Naik, *Biomicrofluidics* **2015**, *9*, 031301.
[34] A. Ullmann, I. Fono, *J. Microelectromech. Syst.* **2002**, *11*, 655.
[35] C. H. Chen, J. G. Santiago, *J. Microelectromech. Syst.* **2002**, *11*, 672.
[36] B. Zhao, J. S. Moore, D. J. Beebe, *Anal. Chem.* **2002**, *74*, 4259.
[37] J. M. Chen, P. C. Huang, M. G. Lin, *Microfluid. Nanofluid.* **2008**, *4*, 427.
[38] L. X. Kong, A. Perebikovsky, J. Moebius, L. Kulinsky, M. Madou, *J. Lab Autom.* **2016**, *21*, 323.
[39] M. Madou, J. Zoval, G. Jia, H. Kido, J. Kim, N. Kim, *Annu. Rev. Biomed. Eng.* **2006**, *8*, 601.
[40] N. R. Glass, R. J. Shilton, P. P. Chan, J. R. Friend, L. Y. Yeo, *Small* **2012**, *8*, 1881.

[41] J. Choi, Y. G. Jung, J. Kim, S. Kim, Y. Jung, H. Na, S. Kwon, *Lab Chip* **2013**, *13*, 280.
[42] D. Brassard, L. Clime, K. Li, M. Geissler, C. Miville-Godin, E. Roy, T. Veres, *Lab Chip* **2011**, *11*, 4099.
[43] J. N. Lee, C. Park, G. M. Whitesides, *Anal. Chem.* **2003**, *75*, 6544.
[44] S. Halldorsson, E. Lucumi, R. Gomez-Sjoberg, R. M. T. Fleming, *Biosens. Bioelectron.* **2015**, *63*, 218.
[45] A. Bietsch, B. Michel, *J. Appl. Phys.* **2000**, *88*, 4310.
[46] D. Y. Khang, H. Q. Jiang, Y. Huang, J. A. Rogers, *Science* **2006**, *311*, 208.
[47] J. C. Lotters, W. Olthuis, P. H. Veltink, P. Bergveld, *J. Micromech. Microeng.* **1997**, *7*, 145.
[48] J. D. Wang, N. J. Douville, S. Takayama, M. ElSayed, *Ann. Biomed. Eng.* **2012**, *40*, 1862.
[49] H. Cho, H. Y. Kim, J. Y. Kang, T. S. Kim, *J Colloid Interface Sci.* **2007**, *306*, 379.
[50] C. P. Huang, J. Lu, H. Seon, A. P. Lee, L. A. Flanagan, H. Y. Kim, A. J. Putnam, N. L. Jeon, *Lab Chip* **2009**, *9*, 1740.
[51] D. T. Eddington, J. P. Puccinelli, D. J. Beebe, *Sens. Actuators, B* **2006**, *114*, 170.
[52] A. A. S. Bhagat, E. T. K. Peterson, I. Papautsky, *J. Micromech. Microeng.* **2007**, *17*, 1017.
[53] H. M. Xia, S. Y. M. Wan, C. Shu, Y. T. Chew, *Lab Chip* **2005**, *5*, 748.
[54] J. Marshall, P. Kupchak, W. M. Zhu, J. Yantha, T. Vrees, S. Furesz, K. Jacks, C. Smith, I. Kireeva, R. Zhang, M. Takahashi, E. Stanton, G. Jackowski, *J. Proteome Res.* **2003**, *2*, 361.
[55] D. Tamburro, C. Fredolini, V. Espina, T. A. Douglas, A. Ranganathan, L. Ilag, W. Zhou, P. Russo, B. H. Espina, G. Muto, *J. Am. Chem. Soc.* **2011**, *133*, 19178.
[56] K. Sato, F. Sato, *Am. J. Physiol.* **1983**, *245*, R203.
[57] P. B. Licht, H. K. Pilegaard, *Ann. Thorac. Surg.* **2004**, *78*, 427.
[58] N. A. Taylor, C. A. Machado-Moreira, *Extreme Physiol. Med.* **2013**, *2*, 4.
[59] F. Costa, D. H. Calloway, S. Margen, *Am. J. Clin. Nutr.* **1969**, *22*, 52.
[60] O. Mickelsen, A. Keys, *J. Biol. Chem.* **1943**, *149*, 479.
[61] R. Peng, Z. Sonner, A. Hauke, E. Wilder, J. Kasting, T. Gaillard, D. Swaille, F. Sherman, X. Mao, J. Hagen, R. Murdock, J. Heikenfeld, *Lab Chip* **2016**, *16*, 4415.